

Rapid eye movement sleep promotes cortical plasticity in the developing brain

Michelle C. Dumoulin Bridi,^{1,2} Sara J. Aton,^{1,3} Julie Seibt,^{1,4} Leslie Renouard,^{1,5} Tammi Coleman,¹ Marcos G. Frank^{1,5*}

2015 © The Authors, some rights reserved; exclusive licensee American Association for the Advancement of Science. Distributed under a Creative Commons Attribution NonCommercial License 4.0 (CC BY-NC). 10.1126/sciadv.1500105

Rapid eye movement sleep is maximal during early life, but its function in the developing brain is unknown. We investigated the role of rapid eye movement sleep in a canonical model of developmental plasticity *in vivo* (ocular dominance plasticity in the cat) induced by monocular deprivation. Preventing rapid eye movement sleep after monocular deprivation reduced ocular dominance plasticity and inhibited activation of a kinase critical for this plasticity (extracellular signal-regulated kinase). Chronic single-neuron recording in freely behaving cats further revealed that cortical activity during rapid eye movement sleep resembled activity present during monocular deprivation. This corresponded to times of maximal extracellular signal-regulated kinase activation. These findings indicate that rapid eye movement sleep promotes molecular and network adaptations that consolidate waking experience in the developing brain.

INTRODUCTION

In humans and other altricial mammals, the amount of rapid eye movement (REM) sleep is much higher in the perinatal period than in adulthood (1). The abundance of REM sleep coincides with developmental periods of heightened synaptogenesis and brain plasticity, suggesting that REM sleep plays a crucial role in cortical maturation (1, 2). This may be especially true during critical periods when the cerebral cortex is sensitive to sensory input (3, 4), as apparent from studies of cortical plasticity *in vitro* (5).

We investigated the function of REM sleep in brain development by exploring its role in ocular dominance plasticity (ODP) in perinatal cats. ODP is a form of cortical plasticity *in vivo* that is triggered by monocular deprivation (MD) during a critical period of development. MD causes individual neurons in primary visual cortex (V1) to shift from being responsive to both eyes to being preferentially responsive to the open (nondeprived) eye (3). Since its original description in the 1960s, ODP has become one of the best studied models of developmental plasticity *in vivo* (6, 7). Therefore, identifying the role of REM sleep in this system may reveal basic rules by which experience and REM sleep shape circuits throughout the developing brain.

RESULTS

We have previously shown that ODP is enhanced by sleep, but the precise role of REM sleep in this process is unknown (4). To specifically probe the role of REM sleep in ODP, we instrumented developing cats for electroencephalographic (EEG) and electromyographic (EMG) recordings and subjected them to the following conditions. Cats received 6 hours of MD while awake, which is sufficient to trigger ODP (4, 8). This was followed by three different manipulations of sleep. One group was allowed undisturbed sleep for 1 hour (sleep group). We awakened the second group when we detected REM sleep,

which began 5 to 10 min after sleep onset [REM sleep deprivation (RSD) group]. We awakened the third group the same number of times, and with the same distribution across the sleep period, but only during non-REM (NREM) sleep [NREM sleep fragmentation (NF) group] (fig. S1B). This is a necessary control because RSD has indirect effects on NREM sleep duration and EEG activity (9). After 6 hours of MD and 1 hour of sleep, whether disrupted or not, we prepared animals for intrinsic signal optical imaging (8) to measure ODP. This imaging approach samples plasticity over large regions of V1. We performed the same three sleep manipulations on a separate set of cats and harvested V1 tissue for Western blot analysis according to previously described methods (8, 10). We were able to control the expression of sleep states as required in our design. REM sleep was significantly reduced in the RSD group relative to the two control groups (undisturbed sleep and NF). Indirect effects of RSD on NREM sleep were reproduced in the NF group. NREM sleep continuity, measured by the length of NREM sleep bouts, was decreased by both RSD and NF (Fig. 1C). There were no differences in how alert the animals were during MD (as measured by EEG slow-wave activity during wake) (fig. S1A). Moreover, stress hormone concentrations (serum cortisol) did not differ across groups (fig. S1D) and were an order of magnitude smaller than levels reported to cause minor impairments in ODP (11).

RSD abolished the normal enhancement of ODP observed after sleep. Cats with normal sleep show shifts in ocular dominance (OD), as previously reported (4). This effect was reduced after RSD yet preserved after NF (Fig. 2). These effects were quantified with scalar measures of ODP on the basis of the responsiveness of each pixel to the nondeprived and deprived eyes. These include the nondeprived eye bias index (NBI) and monocular index (MI), individually calculated for each hemisphere, and the shift index (SI), a measure of plasticity across both hemispheres in the same animal. The NBI ranges from 0 to 1 (0.5 indicates no shift), the MI ranges from 0 to 1 (0 indicates complete binocularity), and the SI ranges from -1 to 1 (0 indicates no shift, and 1 indicates complete dominance by the nondeprived eye). As shown in Fig. 2C, RSD decreased all of these measures compared to those in sleeping animals. Furthermore, the OD shift after RSD was comparable to the shift observed in animals that underwent MD without subsequent sleep (Fig. 2C, reference lines). The OD shift was not impaired in NF animals, demonstrating that the effects of RSD cannot be attributed to indirect effects on other states. These results

¹Department of Neuroscience, Perelman School of Medicine, University of Pennsylvania, Philadelphia, PA 19104, USA. ²Zanvyl Krieger Mind/Brain Institute, Johns Hopkins University, Baltimore, MD 21218, USA. ³University of Michigan, Ann Arbor, MI 48109, USA. ⁴Charité—Universitätsmedizin, Berlin 10117, Germany. ⁵College of Medical Sciences, Washington State University, Spokane, WA 99201, USA.

*Corresponding author. E-mail: marcos.frank@wsu.edu

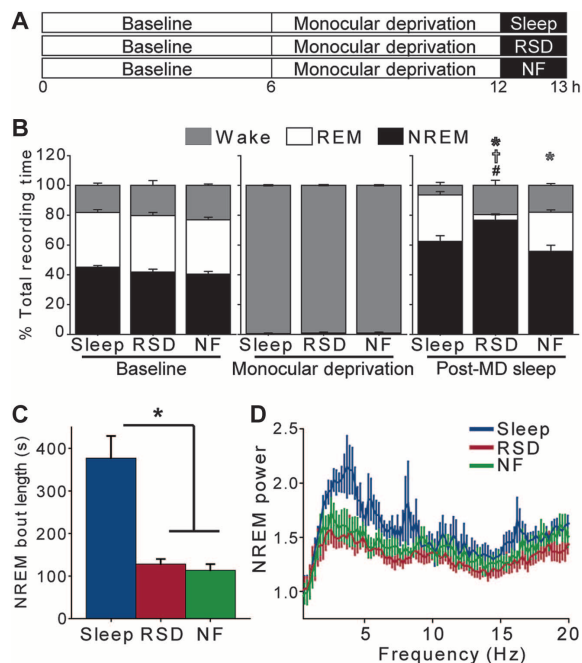


Fig. 1. REM sleep can be selectively deprived in developing cats.

Sleep, $n = 11$; RSD, $n = 12$; NF, $n = 10$. Error bars, SEM. **(A)** Experimental design. We recorded baseline EEG/EMG signals and then performed MD during wake under lighted conditions. Then, we allowed animals 1 hour of sleep, RSD, or NF in complete darkness. **(B)** Time spent in each arousal state during the baseline, MD, and post-MD periods. RSD significantly reduced REM sleep. Both RSD and NF increased post-MD wake time. $*P < 0.05$ (wake); $^{\dagger}P < 0.05$ (REM sleep); $^{\#}P < 0.05$ (NREM sleep), analysis of variance (ANOVA) on ranks followed by Dunn's post hoc test versus sleep group. Sleep, $n = 11$ animals; RSD, $n = 12$; NF, $n = 10$. **(C)** RSD and NF decreased NREM bout duration. $*P < 0.05$, ANOVA on ranks followed by Dunn's post hoc test. Sleep, $n = 11$ animals; RSD, $n = 12$; NF, $n = 10$. **(D)** EEG signals from V1 leads were Fourier-transformed, and the power spectrum during post-MD NREM sleep was normalized to baseline. Mean power in the 0.5- to 4-Hz and 4- to 10-Hz frequency bands did not differ between groups (ANOVA on ranks, $P > 0.06$; sleep, $n = 11$ animals; RSD, $n = 11$; NF, $n = 10$).

were confirmed by electrophysiological single-unit recordings in a subset of animals (fig. S2).

The first 2 hours of sleep after MD (REM + NREM) increases V1 phosphorylation of two kinases implicated in long-term synaptic potentiation: calcium/calmodulin-dependent protein kinase II (CaMKII) and extracellular signal-regulated kinase (ERK) (8). Kinase phosphorylation in V1 requires sleep, because it does not occur in sleep-deprived animals. It also requires the induction of plasticity in prior wake (via MD), because it also does not occur when sleep is instead preceded by equal periods of wakefulness combined with normal vision (8). We have also shown that ERK phosphorylation in sleep is essential for sleep-dependent ODP (10). We found that RSD after MD profoundly and selectively inhibited ERK phosphorylation in V1 (Fig. 3). In contrast, ERK1/2 phosphorylation was normal in the NF group, indicating that this effect is not due to nonspecific effects of RSD on NREM sleep. We also measured levels of cofilin (fig. S3), which is concentrated at excitatory postsynaptic terminals and increased after long-term potentiation protocols (12). Cofilin in V1 was decreased by RSD, but not NF, compared

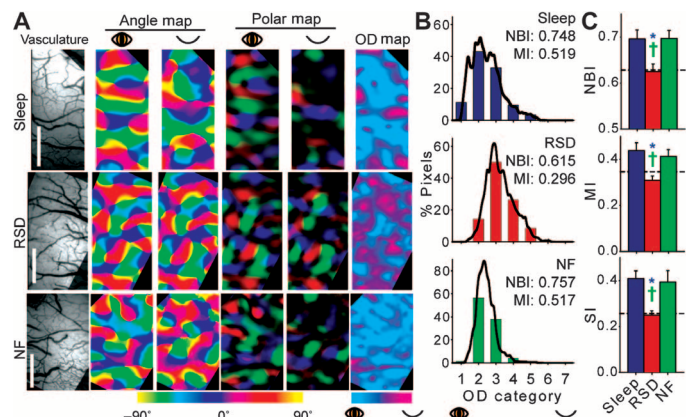


Fig. 2. RSD impairs ODP consolidation. **(A)** Representative optical maps from animals that received sleep, RSD, or NF after MD. Vascular maps show the pial surface of V1, cropped to remove out-of-focus areas and large vessels; scale bar, 1 mm. Angle and polar maps are color-coded to indicate the visual stimulus orientation that maximally drives the response at a given pixel. In polar maps, pixel brightness indicates the magnitude of the response. A polar map that is overall brighter in response to nondeprived than deprived eye stimulation indicates that an OD shift has occurred. This is also shown in the OD ratio maps, which show cortical areas dominated by stimulation of either eye. We quantified this shift by analyzing images pixel by pixel. **(B)** Responses at each pixel in the maps shown in (A) were binned into 70 OD categories on the basis of the ratio of their responsiveness to the nondeprived and deprived eyes (black line). The distribution was collapsed into seven OD categories to produce the classical seven-point scale of Hubel and Wiesel (3). **(C)** Average (\pm SEM) scalar measures of the OD shift. The OD shift after RSD was significantly reduced compared to those after sleep and NF, measured by the NBI ($*P = 0.011$, sleep versus RSD; $^{\dagger}P = 0.009$, NF versus RSD), MI ($*P = 0.003$, sleep versus RSD; $^{\dagger}P = 0.013$, NF versus RSD), and SI ($*P < 0.001$, sleep versus RSD; $^{\dagger}P = 0.034$, NF versus RSD). One-way ANOVA followed by Fisher's least significant difference (LSD) test (30); sleep, $n = 9$ hemispheres; RSD, $n = 10$; NF, $n = 10$. The hashed reference line represents comparable values from animals analyzed after 6 hours of MD only without subsequent sleep [adapted from (8)].

to normally sleeping animals. RSD did not significantly affect CaMKII α / β phosphorylation (Fig. 3) or phosphorylation of the AMPA receptor subunit GluA1 on the CaMKII site (S831; fig. S3). These findings show that after MD, REM sleep is specifically required for ERK activation. They further suggest that NREM sleep is specifically required for CaMKII activation. This is because although RSD is sufficient to reduce ERK phosphorylation, NREM sleep deprivation must also occur for similar reductions in phosphorylated CaMKII (8).

Then, we examined whether these changes were specific to V1 or also occurred in nonvisual cortex. We performed Western blot analysis on primary auditory cortex, primary motor cortex, and lateral cerebellum obtained from the same animals used in the analysis of V1 tissue (fig. S4). The effect of RSD on ERK activation in auditory and motor cortices did not reach significance when these areas were separately analyzed. When the values from auditory and motor cortices were pooled, RSD impaired ERK2 phosphorylation. This suggests that REM sleep may generally promote ERK phosphorylation, but this is intensified in cortical areas undergoing heightened plasticity. RSD had no effect on cerebellar ERK phosphorylation.

Next, we explored the temporal requirement of REM sleep in ODP. First, we addressed whether additional REM sleep after RSD rescued

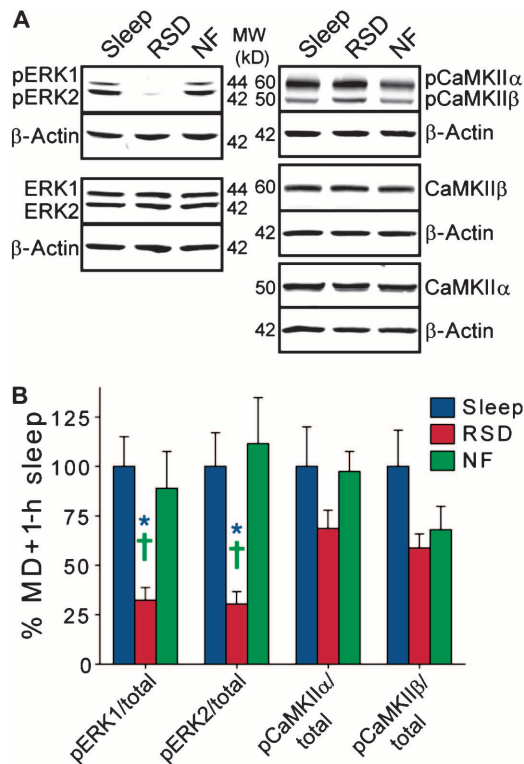


Fig. 3. RSD decreases ERK phosphorylation in V1. (A) Representative Western blots. pERK1, phospho-ERK; pCaMKII α , phospho-CaMKII α . (B) Average (\pm SEM) protein phosphorylation (displayed as percent of sleep group levels). Compared with sleep and NF, ERK1/2 phosphorylation was significantly reduced by RSD. * $P < 0.05$, sleep versus RSD; $^{\dagger}P < 0.05$, NF versus RSD, ANOVA on ranks followed by Dunn's post hoc test. Sleep, $n = 12$ hemispheres; RSD, $n = 14$; NF, $n = 10$.

cortical plasticity. Second, we asked whether REM sleep could protect ODP from subsequent disruption by RSD. To answer these questions, we formed additional groups in which animals received 6 hours of MD during wake. Then, we performed 1-hour RSD followed by 1 hour of undisturbed recovery sleep (RSD + recovery group) or allowed animals 1 hour of undisturbed sleep followed by 1 hour of RSD (delayed RSD group). Because these groups were sampled 2 hours after the MD period ended, they were compared to animals REM sleep-deprived for 2 hours (fig. S5A). For all groups, REM sleep was reduced during the planned RSD period to similar levels (fig. S6). As shown in figs. S5 (B and C) and S6, animals in the RSD + recovery group showed a rebound in REM sleep amounts and greater OD shifts relative to the 2-hour RSD group. This rescue of ODP was paralleled by a rescue of ERK phosphorylation (fig. S7, A and B). We also confirmed that once REM sleep occurred, subsequent RSD did not reduce the OD shift (fig. S5, B and C) or ERK phosphorylation (fig. S7, A and B).

Then, we more closely examined changes in REM sleep architecture that might account for the effects of REM sleep on ODP in animals that received 1 to 2 hours of undisturbed sleep. We observed positive and significant correlations between REM sleep EEG β - γ (20 to 40 Hz) activity in V1 and optical measures of plasticity (the SI) (fig. S8A). V1 β - γ activity was also correlated with ERK1 phosphorylation, although this was not significant for ERK2 phosphorylation (fig. S8B). However, there were no significant correlations between EEG activity in

standard NREM sleep bands and ODP (δ : 0.5 to 4.0 Hz, $P = 0.43$; σ : 12 to 15 Hz, $P = 0.48$) or ERK1 (δ , $P = 0.80$; σ , $P = 0.56$) or ERK2 phosphorylation (δ , $P = 0.91$; σ , $P = 0.68$).

The correlation of REM sleep EEG activity with ODP and ERK phosphorylation prompted us to more closely examine single-neuron activity during this sleep state. For example, in adult rodent hippocampus (13) and visual cortex (14), neuronal activity patterns present during maze running can be detected in subsequent NREM sleep. Similar results in the hippocampus have also been reported during REM sleep in some studies [(15); but see (16)]. In addition, using different analytical techniques and methods, waking patterns of neuronal activity during sleep are reported in song bird nuclei (17) and rodent motor cortex (18). To investigate whether patterns of neuronal activity during MD were present in subsequent REM sleep, we chronically recorded single V1 neurons using stereotrodes in freely behaving cats (19). Single-unit spike trains across the electrode assembly were analyzed with an artificial neural network (ANN) algorithm used in machine learning and pattern recognition (20, 21) (NeuroSolutions version 6.2; NeuroDimensions Inc.). The algorithm was trained to recognize unit activity patterns unique to the MD or baseline binocular vision (pre-MD) period for each animal with 97 to 100% accuracy. Then, the trained network was used to screen each bout of REM sleep binned into 10-s epochs before (baseline pre-MD) or after MD (post-MD). The probability that the pattern of activity in REM sleep matched patterns during MD was higher in REM sleep after MD than before (Fig. 4C). This peaked in the first 2 hours after MD and then declined, paralleling the expression of phosphorylated ERK in V1 (8). Although not identical to "replay" as measured in the hippocampus (13), these results are best explained as a reappearance of waking patterns of cortical activity during REM sleep.

DISCUSSION

In summary, we find that REM sleep plays an important role in enhancing experience-dependent plasticity in the developing cerebral cortex of cats. These findings support a long-standing hypothesis that REM sleep in early life promotes circuit formation (2). Our findings suggest that REM sleep achieves this function by promoting molecular and network events that reinforce neural patterns present during experience. For example, the activation of ERK against a background of waking-like unit activity may lead to the strengthening of selected circuits (10). Our results also further support a role for ERK in ODP, as originally reported in rodents (22).

In contrast with our findings, 1 week of continuous RSD or brainstem lesions that reduce ponto-geniculo-occipital (PGO) waves during REM sleep amplify the effects of MD on cell size in the lateral geniculate nucleus (LGN) of the thalamus (23, 24). There are a number of methodological differences that may account for this apparent discrepancy. In the former studies, sleep or PGO deprivation began 1 week after MD was induced, whereas we examined the immediate effects of short-term MD. In addition, older animals were used in the former study, at ages where the critical period for cortical plasticity is waning. This suggests that REM sleep influences different processes at different phases of the visual critical period. First, cortical activity patterns and ERK activation during REM sleep consolidate experience-dependent plasticity within V1. As the critical period begins to close, REM sleep begins to enforce the normal development of the LGN even when visual experience is altered.

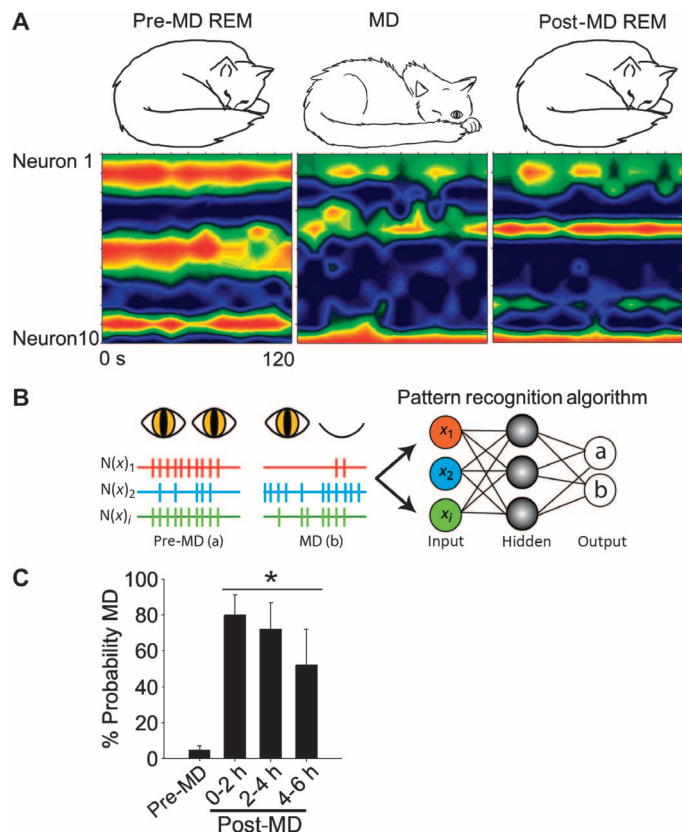


Fig. 4. Patterns of V1 neuronal firing in REM sleep resemble patterns during MD. (A) Heat maps showing patterns of single V1 neuron activity (averaged in 10-s epochs and rank-transformed for display purposes) in a representative, freely moving cat (dark blue, firing rate minima; red, maxima). Data are contiguous 10-s segments of neuronal firing during REM sleep in the normal vision, baseline (pre-MD) period (left panel), MD in the awake animal (middle panel), and in the first hour of post-MD REM sleep (right panel). Each neuron is displayed along the y axis, time is displayed on the x axis, and intensity of unit firing is denoted by changes in color. Note how neuronal activity in REM sleep changes (from pre to post) to resemble activity during MD. (B) Cartoon shows a supervised learning algorithm [multilayer perceptron (MLP) neural network] trained to identify patterns of activity specific to the normal vision period (a) or MD period (b) (with 97 to 100% accuracy) and then used to screen pre-MD or post-MD REM sleep for matches to the MD pattern. The MLP architecture is composed of an input layer [x_1 - x_i , corresponding to firing rates in individual neurons (N_1 - N_i) in the pre-MD waking or MD waking periods], a hidden processing layer, and an output layer. (C) Mean probability that neuronal activity in REM sleep matches activity during MD. Post-MD REM sleep data were divided into 2-hour segments and contained the average value for all bouts ≥ 1 min in length. An equivalent number of bouts (randomly selected) were used for the baseline (pre-MD) REM sleep comparison group. Mean probability of match to MD pattern was significantly higher in post-MD REM sleep than in baseline REM sleep ($n = 5$; $*P < 0.006$ versus baseline, $F = 6.036$, one-way ANOVA).

However, it is likely that both NREM and REM sleep contribute to the development of neural circuits. The amount of NREM sleep positively correlates with ODP (4) and is essential for CaMKII phosphorylation in V1 after MD, a critical enzymatic step in ODP (8). Moreover, N-methyl-D-aspartate (NMDA) receptor blockade across both states inhibits sleep-dependent plasticity and CaMKII and ERK phosphorylation

in V1 (8). NMDA receptor-mediated CaMKII activation may be a prerequisite step for downstream ERK phosphorylation in cortical neurons (25). Thus, we suggest that NMDA receptor activation in each sleep state activates different, but complementary, kinase events, consistent with models reflecting a two-step circuit consolidation process that spans both NREM and REM sleep (26, 27). In particular, our results are consistent with a synaptic consolidation role for REM sleep, as proposed by Diekelmann and Born (27).

Last, our findings raise a number of interesting questions. For example, does REM sleep serve similar functions elsewhere in the developing and adult brain? This possibility is supported by the fact that REM sleep-mediated ERK phosphorylation also occurs in nonvisual cortex (fig. S4) and by the finding that REM sleep influences anatomical changes in the thalamus triggered by MD (23). REM sleep is also important for perceptual learning in adult humans (28). Collectively, these findings suggest that REM sleep may serve similar functions in other parts of the brain and across the life span.

MATERIALS AND METHODS

Study design

The objective of this research was to test the hypothesis that REM sleep is required for ODP consolidation. All animal procedures were approved by Institutional Animal Care and Use Committee of the University of Pennsylvania and performed in accordance with U.S. Department of Agriculture regulations. Kittens were obtained from our on-site breeding colony and housed with their queens on a 12:12 light/dark cycle before experimentation. Animals from the same litter were distributed across groups to control for interlitter variability. Individual animals were randomly assigned to the experimental groups. Sample sizes were chosen on the basis of previous studies from our laboratory (8) and adjusted to achieve minimal statistical power of 0.8. Experiments were performed by nonblinded investigators.

Surgical procedures for polysomnography

Cats within the critical period [about postnatal days (P) 22 to P30] were anesthetized and prepared for surgery as described previously (4, 29). Briefly, the animal was intravenously anesthetized with midazolam and propofol before being intubated and transferred to isoflurane anesthesia. Six EEG and three nuchal EMG electrodes attached to an electrical socket were implanted and affixed to the skull using bone screws and dental acrylic. Two EEG leads were placed over V1 in each hemisphere of animals used for tissue harvesting. We have previously shown that this does not alter cortical concentrations of protein kinases (8). Animals used for imaging had a single EEG lead placed over V1 in each hemisphere to minimize the risk of dimpling the cortical surface with EEG screws. The remaining EEG screws were placed in frontoparietal regions. After at least 4 days of postoperative recovery and treatments, an equal number of male and female animals were randomly assigned to the experiments described below.

Polysomnography and MD

Cats were singly housed in a recording chamber. Mean ages for all animals used in this study at time of MD are shown in tables S1 and S2. The floor of the chamber consisted of a motorized platform that could be activated to awaken the animal. The implanted electrical socket was attached to an electrical cable tether/commutator, which routed

EEG and EMG signals to an amplifier system (Grass Technologies). Signals were high pass-filtered at 0.1 Hz (EEG) or 10 Hz (EMG), low pass-filtered at 100 Hz, digitized at 200 Hz, and recorded using commercial sleep-recording software (VitalRecorder; Kissei Comtec America Inc.). At the end of a baseline recording period lasting at least 6 hours, animals were briefly anesthetized with isoflurane, and the right eyelid was sutured shut. From induction to recovery from anesthesia, this process took no longer than 15 min. After recovery from anesthesia, animals were kept awake for 6 hours under lighted conditions, ensuring that all cats received 6 hours of monocular vision to induce cortical remodeling (4, 29).

Sleep manipulations

After 6 hours of MD, animals were allowed to sleep in complete darkness for 1 to 2 hours. This dark period ensured that visual experience was held constant in all groups after the MD period (4). During the sleep period, the animals underwent one or more of the following manipulations: undisturbed sleep, RSD, or NF. During RSD, the EEG and EMG signals were monitored by an experimenter trained in cat polysomnography (M.C.D.B.). Each time an animal attempted to enter REM sleep based on polysomnographic signals, the animal was awoken by activation of the motorized floor of the chamber (4). During NF, the animals were awoken the same number of times as the RSD animals but only during NREM sleep (RSD: 21.25 ± 1.2 awakenings, $n = 12$; NF: 20.2 ± 0.47 , $n = 10$; $P = 0.428$, t test). The timing of these awakenings was matched to the timing of awakenings in the RSD group as closely as possible (fig. S1). We decided to use only 1 to 2 hours of RSD after the MD period for the following reasons. Earlier studies showed that after 1 to 2 hours of RSD, attempts to enter REM sleep rapidly increased in developing cats (4) (fig. S1). This resulted in a substantial accumulation of REM sleep by the third hour. In addition, even in rare cases where REM sleep could be reduced for longer periods (6 hours), the amount of REM sleep accumulated at the end of an experiment could be substantial (20 to 30 min) (8).

Sleep/wake analysis

Vigilance states were manually scored by a trained experimenter as REM sleep, NREM sleep, or wake in 8-s epochs on the basis of frontoparietal EEG and nuchal EMG signals (SleepSign for Animal; Kissei Comtec America Inc.) according to previously described criteria (8, 29). Percentage of total recording time and average bout duration for each vigilance state was calculated for baseline, MD, and post-MD periods. Fast Fourier transforms were performed on frontoparietal and V1 EEG recordings and normalized to baseline values. One animal in the 1-hour RSD group was excluded from V1 spectral power analysis because the V1 EEG signal was not usable.

Optical imaging of intrinsic cortical signals

ODP was measured by optical imaging of intrinsic cortical signals in 16 male and 15 female cats. Immediately after the sleep period, animals were prepared for optical imaging as previously described (4, 29). Briefly, animals were anesthetized with isoflurane ($\pm N_2O$), and the skull above V1 was removed. The animals were paralyzed with a continuous intravenous infusion of Flaxedil and ventilated. The dura above V1 was removed, and the brain was covered with 3% agarose and a glass coverslip. Eye drops were used to dilate the pupils (1% atropine) and retract the nictitating membranes (10% phenylephrine). Contact lenses focused the eyes on a monitor positioned 40 cm away. A Dalstar 1M30 charge-coupled device camera (Dalsa) was focused 600 μm below

the pial surface with a 135/50-mm lens combination, and the cortex was illuminated with red light. Reflected light was filtered (610 nm), and images were captured (30 frames/s) while presenting one eye at a time with a full-field rotating, drifting square grating (0.2 cycles/°; 2 cycles/s; 1 full rotation/min). Vital signs were monitored throughout imaging to ensure that heart rate and expired CO₂ levels were comparable during left- and right-eye stimulation. Additional details on the imaging procedure can be found in our previously published study (29).

Images were saved after temporal (four-frame) and spatial (2×2 -pixel) binning. Optical maps were generated, cropped to remove vascular artifacts, and analyzed as previously described [for details, see (29)]. Polar optical maps were used to display qualitative changes in eye preference and orientation selectivity under different conditions. Quantitative measures of OD were obtained by a ratio of signal strength in individual maps generated by stimulating either the left or the right eye. The OD ratio at each pixel was calculated as $OD\ ratio = I/(I + C)$, where I is the ipsilateral response and C is the contralateral response. OD ratios were grouped in seven bins, where bin 1 contains pixels most responsive to the eye contralateral to the imaged hemisphere, bin 4 corresponds to pixels responding about equally to either eye, and bin 7 corresponds to pixels mostly responsive to the ipsilateral eye. The number of pixels in each bin was used to calculate scalar measures of ODP (the NBI, MI, and SI) according to previously described methods (8, 29). The NBI ranges from 0 to 1, where higher values indicate a stronger bias for the nondeprived eye. The SI is a measure of overall changes in OD across both hemispheres of an animal, where larger values indicate a greater OD shift. The MI ranges from a value of 0 (indicating that all imaged pixels respond equally to both eyes) to 1 (indicating a complete loss of binocular responses). These values were calculated for all imaged cats. Values from six age-matched cats that underwent MD with no subsequent sleep (MD only), three of which were reproduced with permission from a previous study (8), were used for comparison. Maps from one hemisphere in the MD + 1-hour sleep and one hemisphere in the MD + 2-hour sleep groups were excluded from the analysis because of poor signal quality.

Single-unit recording

The optical data were confirmed in a subset of the animals used for optical imaging [MD + 1-hour sleep, MD + RSD, and MD + NF; $n = 2$ cats (four hemispheres) per group] using single-unit electrophysiological recordings according to previously described methods (8, 29). Briefly, after optical imaging, a 16-electrode array was advanced from the pial surface in V1 in 100- μm steps until stable single-unit recordings were obtained. Visual stimuli (reversing gratings and blank screen) were randomly presented to each eye as described previously (29). For each single neuron, a ratio of the mean number of evoked action potentials (for example, spikes) at the preferred stimulus orientation between the eyes was computed (the deprived/nondeprived eye ratio). Lower scores indicate greater shifts in response in favor of the nondeprived eye (that is, more plasticity). A total of 307, 196, and 373 neurons, respectively, from sleep, RSD, and NF groups were recorded (obtained from a similar number of steps from the pial surface in all hemispheres). These ratios were grouped by condition (RSD, NF, and sleep) and statistically compared using a Kruskal-Wallis ANOVA on ranks, followed by a Dunn's multiple comparison. These statistics were used because the data were nonparametric and because there were not enough hemispheres per group to use scalar measures of OD (for example, the NBI). There was a significant difference in the deprived/nondeprived eye response

ratios across groups (Kruskal-Wallis, $H = 11.91$, degrees of freedom, 2; $P = 0.003$). This reflected a significant decrease in this ratio in the sleep and NF groups versus the RSD group (indicating less plasticity in the RSD group; Dunn's, $P < 0.05$). There was no significant difference between the sleep and NF groups (fig. S2).

Tissue collection and Western blotting

Fourteen male and 12 female cats were randomly assigned to the sleep groups described above for Western blot analysis. Immediately after 1 hour of post-MD sleep, RSD, or NF, animals were anesthetized with isoflurane and sacrificed with an intracardiac injection of pentobarbital/phenytoin. Primary visual, auditory, and motor cortex (V1, A1, and M1, respectively) and lateral cerebellar tissue were rapidly collected from each hemisphere and frozen on dry ice. In one sleep and one RSD animal, only V1 tissue was collected. Whole-tissue extracts were prepared and analyzed as previously described (8). Briefly, tissue was homogenized in lysis buffer (100 mM NaCl, 10 mM $\text{Na}_4\text{P}_2\text{O}_7 \cdot 10\text{H}_2\text{O}$, 10 mM NaPO_4 , 50 mM NaF, 1 mM Na_3VO_4 , 5 mM EDTA, 5 mM EGTA, 1% SDS) containing phosphatase and protease inhibitor cocktails (1:100; Sigma-Aldrich). Cellular debris was removed by centrifugation, and then lysates were boiled for 10 min in gel loading buffer (2.5% SDS). Protein concentration in each sample was determined with a micro-BCA assay (Thermo Scientific). Forty micrograms of protein per well was separated on precast polyacrylamide gels (Bio-Rad) and transferred to nitrocellulose membranes (0.45- μm pore size; Invitrogen). Membranes were blocked in Odyssey blocking buffer at room temperature (Li-Cor) and then incubated overnight at 4°C with primary antibodies diluted in blocking buffer and 0.1% Tween 20 (Sigma-Aldrich). Primary antibodies were raised in rabbit and obtained from Abcam unless otherwise noted; mouse anti- β -actin (1:10,000) (Sigma-Aldrich) was also included with each primary antibody as a loading control. The following primary antibodies were used: anti-ERK1/2 (1:1000) (Cell Signaling Technology), anti-phospho-ERK1/2 (T202/Y204 and T185/Y187, respectively) (1:500) (Cell Signaling Technology), anti-GluA1 (1:900), anti-phospho-GluA1 (S831) (1:200) (Millipore), anti-CaMKII α (1:1500), anti-CaMKII (1:200) (Enzo Life Science Inc.), anti-phospho-CaMKII α/β (T286 and T287, respectively) (1:1000), and anti-cofilin (1:400). Membranes were simultaneously incubated with both fluorescently conjugated goat anti-rabbit and anti-mouse antibodies (Li-Cor) (1:20,000 in blocking buffer/0.1% Tween) at room temperature in the dark for 1 hour and then scanned and quantified with the Odyssey infrared scanner and quantification software (Li-Cor). Blots were scanned at 700 nm to detect the β -actin loading control and 800 nm to detect each protein of interest. Variation across gels was controlled for by normalizing to a common sample run on multiple gels. Cofilin blots were not run for one animal in the 1-hour sleep and one animal in the 1-hour RSD groups, because not enough protein was obtained.

Stereotrode, chronic recording in freely behaving cats

Data were obtained from five animals used in a previous study [see (19) for details on all procedures]. Briefly, P20 to P25 cats were surgically implanted with stereotrode microdrives (within the medial bank of V1) and nuchal EMG wires. After 4 to 5 days of postoperative recovery and treatments, animals were placed in individual lightproof chambers. Then, 1 to 2 days were used to slowly advance the stereotrodes until stable recordings were obtained. Therefore, these animals were at similar ages as the cats used for optical imaging and protein measurements, before MD was performed. They were housed under normal illumina-

tion, except for the post-MD period when they were maintained in complete darkness to control for additional visual input. Electrophysiological signals were continuously collected using Plexon/RASPUTIN hardware and software, and single-units were isolated using cluster cutting as described previously (19). After a baseline period, one eye was closed using a soft eye patch affixed with tape. During this MD period, the cats were kept awake through play and movement of the cage floor. Only neurons that were held across the 6- to 12-hour baseline, 6-hour MD, and 6-hour post-MD sleep period were used for analyses. A total of 71 neurons met these criteria [54 regular spiking, 16 fast spiking (putative inhibitory interneurons), and 1 intrinsically bursting; mean units per animal, 14.2]. Then, single-unit data were parsed into individual bouts of REM sleep, NREM sleep, and wakefulness as previously described (19).

Detection of neural patterns of activity

Different approaches have been used to detect patterns of waking neural activity during sleep (13, 14, 17, 18). For example, studies of the rodent hippocampus typically use well-rehearsed motor tasks and analyses designed to detect ordered patterns of firing (in cells with spatial receptive fields) repeatedly activated during the task [for example, running on a circular maze (13, 14)]. In our experiments, a different approach was selected because the activity of V1 neurons in a freely behaving animal scanning a complex visual environment is likely to be much more stochastic. In addition, stereotrodes were placed “blind” in the medial bank, and therefore, in any given assembly, recordings could span different functional domains (for example, OD or orientation). This would make it exceedingly unlikely that V1 neurons in our ensembles would be activated in the same stereotyped way across waking experience. Therefore, we used an analytical approach specifically designed to detect patterns in noisier, complex signals. For this reason, we do not refer to our results as replay or “reactivation” to avoid confusion with what these terms refer to in previous studies.

We used an ANN based on the “MLP” to detect different patterns of V1 unit activity. The building block of the MLP is the individual perceptron, which produces a single output from multiple inputs (for example, mean spike rates) by creating a linear combination based on the input weights, followed by processing by a nonlinear activation function. In the MLPs used here, a logistic sigmoid function was used. The perceptron can be represented as follows:

$$y = \left(\sum_{i=1}^n w_i x_i + b \right) = \phi(w^T x + b)$$

where w refers to the vector of weights, x is the vector of inputs, b is the bias (a constant), and ϕ refers to the activation function. Individual perceptrons (or “sigmoid neurons”) can be assembled into a larger array (the MLP), which increases the functionality of the ANN, as the output of each perceptron is fed forward to the next layer (see Fig. 4B). For more details, see (20, 21).

The performance of the ANN MLP in the test samples across five cats ranged from 97 to 100% accuracy in classifying epochs as derived from either the MD or baseline waking periods (see tables S3 and S4 for results of training and testing in a representative animal). Following successful testing, the ANN MLP was used to analyze all REM sleep bouts ≥ 1 min in length in the post-MD sleep period (segmented into 2-hour bins). This was done to maximize the amount of REM sleep data presented to the ANN MLP and to ensure that the state of

REM sleep was sustained long enough for an accurate sampling of ongoing neuronal activity. An equal number of REM sleep bouts of similar lengths were randomly selected from the baseline period to match the number analyzed in each post-MD 2-hour bin. A total of 127 bouts were analyzed from the five cats (baseline: 28, post-MD hours 1 and 2: 32, post-MD hours 3 and 4: 37, and post-MD hours 5 and 6: 30). We computed the mean probability of match (as a percentage) with the MD pattern in each time bin. In a subset of animals, we performed additional pilot studies to verify that the ANN MLP was sensitive to the MD pattern. Varying the number of hidden layers did not appreciably increase the accuracy of the ANN. Shorter or longer segments of spiking activity also did not improve the performance of the ANN. The accuracy of the MLP was also not affected by artificially doubling or halving spike rates, and randomly generated integer values with similar ranges as raw spike data (for example, “fake spikes”) produced very low agreement with the MD pattern (<2%). We also determined whether the % agreement varied within a given bout of REM sleep. However, other than a trend for a drop toward baseline values across the 6-hour post-MD period, there were no significant changes across a given bout of REM sleep at either 1- or 10-s resolution. We also examined neuronal activity at a millisecond scale using cross-correlogram analysis and by examining all pairwise correlations across a given assembly (at a 1- and 10-s scale). However, except for previously reported changes in fast- and regular-spiking neurons (19), no other features of MD activity were detected during sleep using these additional analyses.

Cortisol measurements

Cortisol was measured in a subset of cats in the optical imaging and tissue collection groups. Whole blood was collected from the jugular vein of awake cats at the indicated time points, and Normosol-R was administered subcutaneously to replace fluid volume. Blood was allowed to clot at 4°C and then spun at 2500 rcf for 7 min. Serum was collected and stored at -20°C until analysis. Cortisol was quantified by a solid-phase competitive enzyme-amplified chemiluminescence immunoassay on the Immulite 2000 (Siemens) at the Matthew J. Ryan Veterinary Hospital of the University of Pennsylvania. Cortisol levels below the detection limit of the assay (1 µg/dl) were assigned a value of 1.

Correlation analysis

In animals receiving 1 to 2 hours of ad lib sleep, we performed correlation analysis between sleep architecture and sleep EEG parameters and the OD shift or ERK phosphorylation levels. For both REM and NREM sleep, post-MD EEGs were Fourier-transformed, and the resulting spectral power was averaged in classic bandwidths [σ (12 to 15 Hz), δ (0.5 to 4.0 Hz), θ (5 to 8 Hz), and β - γ (20 to 40 Hz)] and normalized to baseline values. As described above, imaged cats were implanted with a single EEG electrode in each V1 hemisphere, and this bipolar electrode pair was used to obtain the V1 EEG signal. Therefore, correlations on imaged cats were performed between V1 EEG power across both hemispheres and the SI, a measure of plasticity across both hemispheres. We were able to obtain an SI value from seven of the nine imaged sleeping animals, and these values were used in the correlation analysis. Cats used for protein quantification were implanted with a bipolar pair of electrodes in each V1 hemisphere. Fifteen of the recorded hemispheres had unihemispheric EEG recordings. One EEG recording was excluded because of poor signal quality. The remaining 14 hemispheres were used

in the correlation analysis. V1 EEG spectral power was averaged as described above and then correlated with V1 ERK phosphorylation in the same hemisphere.

Statistical analysis

Statistical tests were performed using SigmaPlot 11.0 (Systat Software Inc.). Groups were compared using Student's *t* tests or one-way ANOVAs, as indicated. Fisher's LSD test was used for post hoc analyses in which only three groups were compared (30); the Holm-Sidak post hoc test was used in cases where more than three groups were compared. Correlation analysis was performed using the Pearson product moment correlation. Nonparametric tests (Mann-Whitney *U* tests and ANOVAs on ranks with Dunn's post hoc tests) were used in cases where data were not normally distributed. NeuroSolutions version 6.2 (NeuroDimensions Inc.) was used for all ANN MLP analyses. Each hemisphere was treated as an independent sample, as described previously (8). Data were excluded in the following cases. Optical maps were excluded in the event of poor signal quality. EEG data were excluded if the signals were dominated by movement artifacts or other sources of electrical noise. Grubbs's test was used to detect outliers, and one outlier was removed from the EEG correlation analysis.

SUPPLEMENTARY MATERIALS

Supplementary material for this article is available at <http://advances.sciencemag.org/cgi/content/full/1/6/e1500105/DC1>

- Fig. S1. MD, serum cortisol levels, and timing of awakenings are similar across groups and magnitude of RSD effect comparable to pharmacological block of plasticity.
- Fig. S2. Single-unit recordings in V1 confirm the results from optical imaging.
- Fig. S3. RSD decreases cofilin levels, but not GluA1 phosphorylation, in V1.
- Fig. S4. RSD reduces ERK phosphorylation in nonvisual brain regions.
- Fig. S5. REM sleep in the first 2 hours after MD rescues and protects ODP from further disruption.
- Fig. S6. REM sleep is selectively reduced in the 2 hours after MD.
- Fig. S7. ERK phosphorylation is normal in the RSD + recovery and delayed RSD groups.
- Fig. S8. EEG activity in REM sleep correlates with ODP and ERK phosphorylation.
- Table S1. Numbers and ages of animals used in the 1-hour groups.
- Table S2. Numbers and ages of animals used in the 2-hour groups.
- Table S3. Training and cross-validation of an ANN using the MLP architecture.
- Table S4. Testing and performance of an ANN using the MLP architecture.

REFERENCES AND NOTES

1. M. G. Frank, in *Sleep: Circuits and Functions*, P.-H. Luppi, Ed. (CRC Press, Boca Raton, FL, 2005), pp. 177–192.
2. H. P. Roffwarg, J. N. Muzio, W. C. Dement, Ontogenetic development of the human sleep-dream cycle. *Science* **152**, 604–619 (1966).
3. D. H. Hubel, T. N. Wiesel, The period of susceptibility to the physiological effects of unilateral eye closure in kittens. *J. Physiol.* **206**, 419–436 (1970).
4. M. G. Frank, N. P. Issa, M. P. Stryker, Sleep enhances plasticity in the developing visual cortex. *Neuron* **30**, 275–287 (2001).
5. J. P. Shaffery, C. M. Sinton, G. Bisette, H. P. Roffwarg, G. A. Marks, Rapid eye movement sleep deprivation modifies expression of long-term potentiation in visual cortex of immature rats. *Neuroscience* **110**, 431–443 (2002).
6. D. Tropea, A. Van Wart, M. Sur, Molecular mechanisms of experience-dependent plasticity in visual cortex. *Philos. Trans. R. Soc. Lond. B. Biol. Sci.* **364**, 341–355 (2009).
7. G. B. Smith, A. J. Heynen, M. F. Bear, Bidirectional synaptic mechanisms of ocular dominance plasticity in visual cortex. *Philos. Trans. R. Soc. Lond. B. Biol. Sci.* **364**, 357–367 (2009).
8. S. J. Aton, J. Seibt, M. Dumoulin, S. K. Jha, N. Steinmetz, T. Coleman, N. Naidoo, M. G. Frank, Mechanisms of sleep-dependent consolidation of cortical plasticity. *Neuron* **61**, 454–466 (2009).
9. T. Endo, B. Schwierin, A. A. Borbély, I. Tobler, Selective and total sleep deprivation: Effect on the sleep EEG in the rat. *Psychiatry Res.* **66**, 97–110 (1997).

10. M. C. Dumoulin, S. J. Aton, A. J. Watson, L. Renouard, T. Coleman, M. G. Frank, Extracellular signal-regulated kinase (ERK) activity during sleep consolidates cortical plasticity in vivo. *Cereb. Cortex* **25**, 507–515 (2015).
 11. N. W. Daw, H. Sato, K. Fox, T. Carmichael, R. Gingerich, Cortisol reduces plasticity in the kitten visual cortex. *J. Neurobiol.* **22**, 158–168 (1991).
 12. V. Fedulov, C. S. Rex, D. A. Simmons, L. Palmer, C. M. Gall, G. Lynch, Evidence that long-term potentiation occurs within individual hippocampal synapses during learning. *J. Neurosci.* **27**, 8031–8039 (2007).
 13. M. A. Wilson, B. L. McNaughton, Reactivation of hippocampal ensemble memories during sleep. *Science* **265**, 676–679 (1994).
 14. D. Ji, M. A. Wilson, Coordinated memory replay in the visual cortex and hippocampus during sleep. *Nat. Neurosci.* **10**, 100–107 (2007).
 15. K. Louie, M. A. Wilson, Temporally structured replay of awake hippocampal ensemble activity during rapid eye movement sleep. *Neuron* **29**, 145–156 (2001).
 16. H. S. Kudrimoti, C. A. Barnes, B. L. McNaughton, Reactivation of hippocampal cell assemblies: Effects of behavioral state, experience and EEG dynamics. *J. Neurosci.* **19**, 4090–4101 (1999).
 17. A. S. Dave, D. Margoliash, Song replay during sleep and computational rules of sensorimotor vocal learning. *Science* **290**, 812–816 (2000).
 18. G. Yang, C. S. W. Lai, J. Cichon, L. Ma, W. Li, W.-B. Gan, Sleep promotes branch-specific formation of dendritic spines after learning. *Science* **344**, 1173–1178 (2014).
 19. S. J. Aton, C. Broussard, M. Dumoulin, J. Seibt, A. Watson, T. Coleman, M. G. Frank, Visual experience and subsequent sleep induce sequential plastic changes in putative inhibitory and excitatory cortical neurons. *Proc. Natl. Acad. Sci. U.S.A.* **110**, 3101–3106 (2013).
 20. R. Lippman, An introduction to computing with neural nets. *IEEE Trans. ASSP* **4**, 4–22 (1987).
 21. S. Haykin, *Neural Networks: A Comprehensive Foundation* (Prentice-Hall, Englewood Cliffs, NJ, ed. 2, 1998).
 22. G. Di Cristo, N. Berardi, L. Cancedda, T. Pizzorusso, E. Putignano, G. M. Ratto, L. Maffei, Requirement of ERK activation for visual cortical plasticity. *Science* **292**, 2337–2340 (2001).
 23. A. Oksenberg, J. P. Shaffery, G. A. Marks, S. G. Speciale, G. Mihailoff, H. P. Roffwarg, Rapid eye movement sleep deprivation in kittens amplifies LGN cell-size disparity induced by monocular deprivation. *Dev. Brain Res.* **97**, 51–61 (1996).
 24. J. P. Shaffery, H. P. Roffwarg, S. G. Speciale, G. A. Marks, Ponto-geniculo-occipital-wave suppression amplifies lateral geniculate nucleus cell-size changes in monocularly deprived kittens. *Brain Res. Dev. Brain Res.* **114**, 109–119 (1999).
 25. F. El Gaamouch, A. Buisson, O. Moustié, M. Lemieux, S. Labrecque, B. Bontempi, P. De Koninck, O. Nicole, Interaction between α CaMKII and GluN2B controls ERK-dependent plasticity. *J. Neurosci.* **32**, 10767–10779 (2012).
 26. A. Giuditta, M.V. Ambrosini, P. Montagnese, P. Mandile, M. Cotugno, G. Grassi Zucconi, S. Vescia, The sequential hypothesis of the function of sleep. *Behav. Brain Res.* **69**, 157–166 (1995).
 27. S. Diekelmann, J. Born, The memory function of sleep. *Nat. Rev. Neurosci.* **11**, 114–126 (2010).
 28. A. Karni, D. Tanne, B. S. Rubenstein, J. J. M. Askenasy, D. Sagi, Dependence on REM sleep of overnight improvement of a perceptual skill. *Science* **265**, 679–682 (1994).
 29. S. K. Jha, B. E. Jones, T. Coleman, N. Steinmetz, C.-T. Law, G. Griffin, J. Hawk, M. G. Frank, Sleep-dependent plasticity requires cortical activity. *J. Neurosci.* **25**, 9266–9274 (2005).
 30. J. C. Hsu, *Multiple Comparisons: Theory and Methods* (Chapman & Hall/CRC, Boca Raton, FL, 1996).
- Acknowledgments:** We thank M. Kelz and D. Raizen for constructive comments. **Funding:** This work was supported by departmental funds from the University of Pennsylvania and NIH (EY019022 and HL114161 to M.G.F. and F31NS067935 and T32-HL007713-16 to M.C.D.B.). **Author contributions:** M.C.D.B. performed experiments and analyses and prepared figures and the manuscript. S.J.A. performed chronic unit recordings. J.S. and L.R. assisted with experiments. M.G.F. assisted with analyses and preparation of the manuscript. **Competing interests:** The authors declare that they have no competing interests.
- Submitted 9 February 2015
 Accepted 28 April 2015
 Published 3 July 2015
 10.1126/sciadv.1500105
- Citation:** M. C. Dumoulin Bridi, S. J. Aton, J. Seibt, L. Renouard, T. Coleman, M. G. Frank, Rapid eye movement sleep promotes cortical plasticity in the developing brain. *Sci. Adv.* **1**, e1500105 (2015).

Rapid eye movement sleep promotes cortical plasticity in the developing brain

Michelle C. Dumoulin Bridi, Sara J. Aton, Julie Seibt, Leslie Renouard, Tammi Coleman and Marcos G. Frank

Sci Adv 1 (6), e1500105.

DOI: 10.1126/sciadv.1500105

ARTICLE TOOLS

<http://advances.sciencemag.org/content/1/6/e1500105>

SUPPLEMENTARY MATERIALS

<http://advances.sciencemag.org/content/suppl/2015/06/30/1.6.e1500105.DC1>

REFERENCES

This article cites 27 articles, 11 of which you can access for free
<http://advances.sciencemag.org/content/1/6/e1500105#BIBL>

PERMISSIONS

<http://www.sciencemag.org/help/reprints-and-permissions>

Use of this article is subject to the [Terms of Service](#)

Science Advances (ISSN 2375-2548) is published by the American Association for the Advancement of Science, 1200 New York Avenue NW, Washington, DC 20005. The title *Science Advances* is a registered trademark of AAAS.

Copyright © 2015, The Authors